Stress/strain effects on electrochemical activity: Metallurgical / mechanical interactions and surface reactivity

Halina Krawiec, Vincent Vignal

Stress/strain effects on electrochemical activity: Metallurgical/mechanical/ interactions and surface reactivity

2

Halina Krawiec[a], *Vincent Vignal*[b]
[a]AGH—University of Science and Technology, Faculty of Foundry Engineering, Krakow, Poland, [b]Laboratoire Interdisciplinaire Carnot dee Bourgogne (ICB), UMR 6303 CNRS—Université de Bourgogne-Franche-Comté, Cedex, France

2.1 Introduction

Investigating the tribological contact and sliding between two materials is complicated by the fact that the interface is buried from view and inaccessible to conventional experimental tools. In addition, the tribological contact and sliding of materials is a complex and dynamic system impacted by many factors. They involve from macro to the atomic scale, material transfer, heating, and combination of spatially and temporally varying loads. These loads may be triaxial/biaxial/uniaxial (tensile or compressive), or rotational (strength shear). Stresses and strains may develop within the system. The tribological contact and the sliding of materials can also induce phase transformation due to deformation, formation of point and linear defects (voids, cracks, and scratches), and so on.

In an aggressive environment as in tribocorrosion, the physical-mechanical processes mentioned above are affected by corrosion and vice versa. Therefore, the effect of stress and strain on the electrochemical behavior of metallic surfaces needs to be considered and quantified.

The influence of mechanical loads on cathodic (reduction reactions) and anodic processes (dissolution for instance), as well as on the stability and modifications of passive films are discussed in this chapter. The thermokinetic approach is not discussed and readers interested in thermokinetic formalisms are referred to reference [1].

2.2 Definition of a relevant approach

Numerous factors can affect the reactivity of metallic surfaces. Under certain conditions, synergistic effects between two or more factors can also be observed at different scales. Possible factors include:

- Surface roughness (or surface microroughness),
- Crystallographic texture and grain size,
- Chemical composition (alloying elements, for instance),

Mechanical and Electro-chemical Interactions under Tribocorrosion, https://doi.org/10.1016/B978-0-12-823765-6.00002-X

- Stress/strain. They can be residual fields or applied (external) loads,
- Point and linear defects (scratches, steps, particles, and inclusions),
- Passive films/coatings/contaminants (lubricant and grease).

It is therefore important to first use a statistical approach (Pearson matrix [2], ANOVA module, for example) to determine the parameters whose influence is of order 1 in the given conditions.

Once the most influent parameters are defined, a relevant experimental approach must be selected to study the role of stress/strain. In particular, it must be ensured that the response of the studied system is not significantly affected by factors other than mechanical factors (stress/strain). For example, the influence of surface roughness must be taken into account when studying the role of deformation on reactivity using different surface preparations (mechanical grinding/polishing and electrolytic polishing). Different surface finishes [3] can be used to generate stress/strain fields in alloys like machining, grinding, mechanical polishing, burnishing, and sandblasting. Important is that compressive or tensile stresses can be present on material surfaces.

2.3 Influence of compressive stresses

Experimental techniques used to study the influence of compressive stresses on corrosion (and tribocorrosion) mechanisms will be relevant if they make it possible to generate compressive stresses in a material with negligible work hardening rate, and not inducing changes in (micro)structure and surface roughness. Examples of techniques used to generate compressive stresses are:

- laser shock processing (LSP) [4] applied, e.g., to aluminum alloys [5–7], austenitic and martensitic stainless steels [8], duplex stainless steels [9], nickel alloys [10], and brass [11].
- low plastic burnishing used on AA2024-T3 aluminum alloy [12] and Ca-Mg biomedical alloys [13].

Interested readers are referred to a review paper [14] describing different techniques that can be used to generate compressive stresses. Table 2.1 gives some examples of residual compressive stresses in alloys generated by various techniques.

In all the cases studied, it appears that compressive stresses affect the electrochemical processes and increase the corrosion resistance of metallic alloys. They reduce significantly the kinetics of reduction reactions and the current density in the passive plateau (anodic domain). They can also delay pit initiation and reduce the kinetics of dissolution.

For example, the polarisation behavior of 316L stainless steel in Hank's solution is affected by laser shock peening [15]. Indeed, in the presence of compressive stresses induced by the laser shock (see a red curve in Fig. 2.1), the current density

Table 2.1

Table 2.1 Examples of residual compressive stresses induced in metallic alloys using different techniques.

Alloys	Residual stress value (MPa)	Techniques	References
Friction stir welded AA7075	−80 −120	Laser peening Shot peening	[5]
AA2050-T8	−165	Laser peening	[7]
Duplex stainless steel UNS S31803	−155 (γ-phase) −446 (α-phase)	4000 grit surface finish	[9]
Austenitic stainless steel 316L	−257	Rubber polisher #240	[3]
Brass 260 Brass 280	−140 −107	Laser shock processing	[11]
AA2024-T3	−340	Low plastic burnishing	[12]
Magnesium-calcium implants	[−70; −90]	Low plastic burnishing	[13]

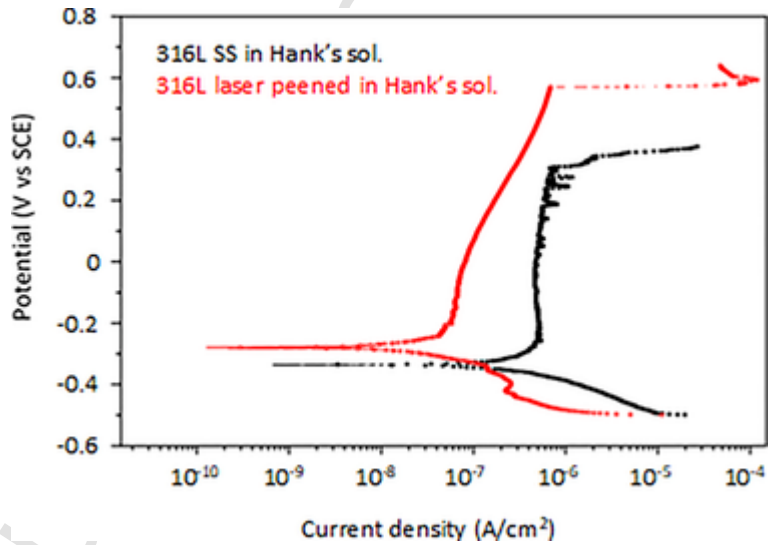

Fig. 2.1 Comparison of the polarisation curves recorded on unpeened *(black curve)* and laser shock peened *(red curve)* 316L stainless steel in Hank's solution.
According to R.K. Gupta, N. Prasad, A.K. Rai, R. Biswal, R. Sundar, A. Bose, P. Ganesh, K. Ranganathan, K.S. Bindra, R. Kaul, Corrosion study on laser shock peened 316L stainless steel in simulated body fluid and chloride medium, Lasers Manuf. Mater. Process. 5 (2018) 270–282.

in the cathodic branch of the polarization curve slightly decreases and the current density in the passive range drops by one order of magnitude. In addition, no metastable pits are observed after polarisation in the passive range of the laser peened sample. The pitting potential of a laser peened sample shifts to more noble values: a difference of about 150 mV is noticed between unpeened and laser peened samples.

The mechanisms responsible for the improvement in corrosion resistance due to compressive stresses are still under debate. The beneficial influence of compressive stresses cannot be explained considering the density of dopants in the passive films. Indeed, it was shown on 316L stainless steel [16] that the density of dopants (both *n*- and *p*-types) is not affected by changing the level of compressive stresses. Some explanations can be found in surface analyses of passive films. Auger measurements were performed after immersion of different stainless steels (302 [17] and 316 [18]) in 1M H_2SO_4 for 20 min. Two samples were considered: a reference sample (no stress) and a sample under compression (generated by bending). Obtained results revealed that the passive film formed in the presence of a compressive stress field is slightly thinner than that formed on the reference surface (thickness of 3.5 nm under compression and 4 nm on the stress-free surface). The passive film formed under compression is also richer in chromium in its inner part than the passive film formed on the reference surface. Fig. 2.2B shows the existence of a peak in the chromium profile of the sample under compression, between 300 and 700 s. Such a peak is not visible on the reference sample (Fig. 2.2A). The protective properties of passive films are usually attributed to the formation of chromium-based compounds in their inner part.

The residual stress field is usually highly heterogeneous in alloys. The relationships between the passive film composition (determined from Auger electron spectroscopy measurements), local residual stresses in the substrate (calculated using a thermal-mechanical simulation based on XRD measurements), and the local electrochemical behavior (via the measurement of the local corrosion potential using microcapillary-based experiments) were studied at the microscale [19]. It was shown that there is a linear relationship between the local corrosion potential and the ratio Cr/Fe in the passive film and between the local corrosion potential and the local residual stress in the substrate. The corrosion potential becomes nobler with increasing compressive stresses in the substrate and with increasing Cr/Fe in the passive film. It was then proposed that the passive film formed on sites under compression is enriched in Cr. This study confirms previous those obtained on 302 and 316 stainless steel (previous paragraph).

The influence of an LSP treatment on the polarisation curve of aluminum alloy AA2050-T8 recorded in 0.1M NaCl at 25°C is shown in Fig. 2.3A [7]. After LSP, similar results to those obtained on stainless steels were found. A drop of the current density is observed both in the cathodic and anodic domains. The pitting potential is also shifted to more noble values. AFM observations show that after LSP only pitting corrosion occurs (Fig. 2.3B), whereas both pitting and intergranular corrosion were found after polishing (Fig. 2.3C). Pitting corrosion occurs in sites containing inter-

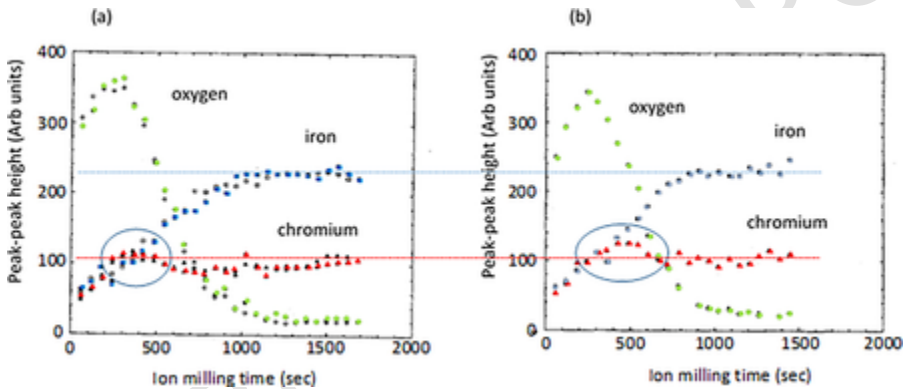

Fig. 2.2 Auger profiles of oxygen, chromium, and iron (ion milling rate of 0.48 nm/min equiv. Si) on: (A) polished sample (no stress, two experiments performed) and (B) sample under compression.
According to F. Navai, J. Mater. Sci. 30 (1995) 1166–1172.

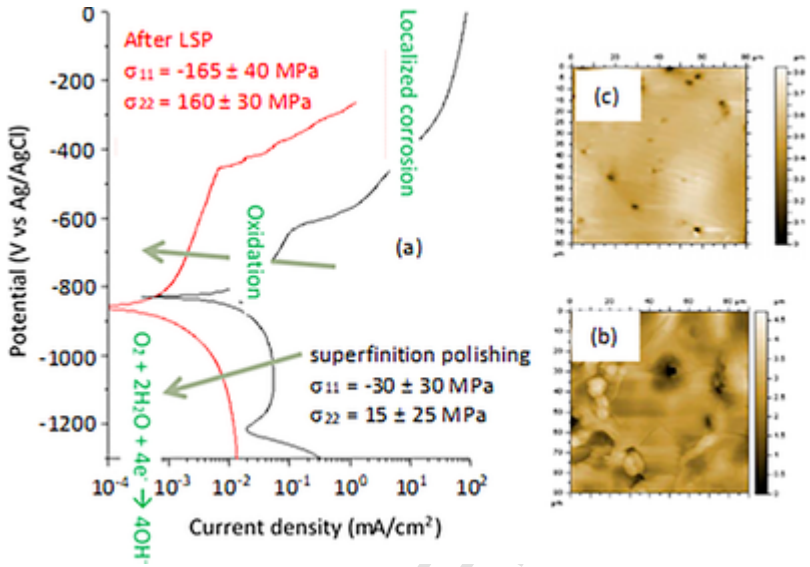

Fig. 2.3 (A) Polarisation curves of AA2050-T8 in 0.1M NaCl at 25°C after either mechanical polishing or LSP. AFM images after corrosion tests (in tapping mode) on (B) LSP treated and (C) mechanical polished aluminium.
According to H. Amar, V. Vignal, H. Krawiec, C. Josse, P. Peyre, S.N. da Silva, L.F. Dick, Corros. Sci. 53 (2011) 3215–3221.

metallic particles due to a galvanic coupling between particles and matrix. No clear explanation was proposed to explain changes detected in the corrosion behavior of aluminum alloys.

Corrosion processes and mechanisms are strongly associated with surface electronic structures such as electron work function (EWF). EWF is the minimum work needed to extract electrons from the Fermi level of a metal/alloy across a surface carrying no net charge. This parameter is highly sensitive to surface conditions (roughness, passive film, stress, strain, and defects). Several papers revealed that EWF is affected by stress/strain [20–25] and a few of these papers [24, 25] showed that compressive stress increases the EWF. The higher the EWF value, the more stable the surface and therefore the higher the corrosion resistance. Recent progress in understanding the corrosion behavior of metallic alloys using SKP can be found in reference [26]. Regarding tribocorrosion, it was underlined that some surface properties, such as adhesion and friction, are largely influenced by surface electron activity, which can be reflected by EWF [27]. Relevant experiments [28] have demonstrated a close correlation between EWF and adhesive force for surfaces in contact.

The beneficial effect of compressive stresses on the corrosion behavior of metallic materials is however not a general rule. Indeed that may be the case when other facts appear simultaneously with the development of compressive stresses like the

formation of both a rough surface and a cold worked layer (plastic deformation) near the surface as in the case of alloy 800 [29] and the decohesion of the surface layer in the case of carbon steel [30].

2.4 Influence of tensile stresses in the elastic domain

The transition between domains where compressive and tensile stresses exist is very important since, at that transition, the corrosion resistance of metallic alloys decreases. This is the case for duplex stainless steels in sodium chloride solutions [9] The time to a pit of UNS S31803 duplex stainless steel was measured vs. applied stress (located in the elastic domain), as shown in Fig. 2.4. Experiments were performed in 0.5M NaCl at 50°C, under potentiostatic conditions (at 300 and 400 mV vs SCE). Surface stresses were also measured by means of XRD in both phases. Two domains are visible. In domain I, eight experiments (of the 10 experiments performed) leads to passive behavior (no time to pit identified within 100 h). By contrast, only three experiments (of the 10 tests performed) leads to passive behavior in domain II. At the transition between the two domains, a drop in the corrosion resistance is observed. Residual stress measurements (using XRD) showed that this transition corresponds to the transition from compressive to tensile stresses in the austenite phase (the ferrite phase being under compression in both domains).

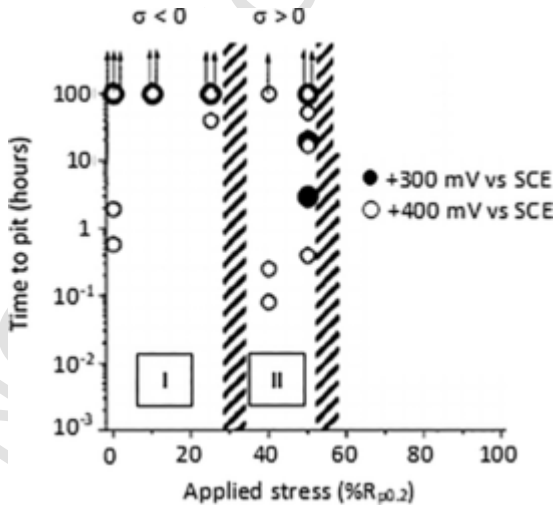

Fig. 2.4 Evolution of the time to pit vs applied stress for UNS S31803 duplex stainless steel in 0.5M NaCl at 50°C, under potentiostatic conditions.
According to V. Vignal, N. Mary, C. Valot, R. Oltra, L. Coudreuse, Electrochem. Solid-State Lett. 7 (2004) C39–C42.

The deleterious influence of tensile stresses on the electrochemical behavior and corrosion resistance was also reported for the following metallic alloys, namely 316L stainless steel [16], ferritic steel [31], 304L stainless steel [32, 33], high-strength galvanized steel [34], carbon steel [35], X80 steel [36], aluminum alloys 7075 [37] and 7010 [38], Fe-based amorphous coatings [39], and 316L stainless steel [40]. Table 2.2 gives some examples of tensile residual stresses generated in metallic alloys using various techniques.

The experimental techniques used to induce tensile stresses in the elastic domain are relevant when they generate tensile stresses in the material with a negligible work hardening rate, and with no change neither in (micro) structure or surface roughness. This is illustrated in Fig. 2.5 showing the effect of stresses induced by mechanical loadings at different levels on the cyclic voltammograms recorded on carbon steel immersed in simulated concrete pore solutions containing either or not chloride ions [35]. The peaks observed on these voltammograms correspond to the oxidation or re-
Table 2.2

Table 2.2 Examples of residual tensile stresses induced in alloys using different techniques.

Metals and alloys	Residual stress value (MPa)	Techniques	References
High-strength structural steel	+190	Tempering at 100°C (30 min)	[41]
5A12 aluminum alloy	[+50; +110]	Nd: YAG laser cleaning (50–110 W)	[42]
High strength alloy steel	[+600; +800]	Machining	[43]
40Cr	+70	Ultrahigh speed grinding	[44]
Austenitic stainless steel 316L	+19	Electropolishing	[3]
	+315	Angle grinder	
X65 steel (weld zone)	+160	Welding	[45]

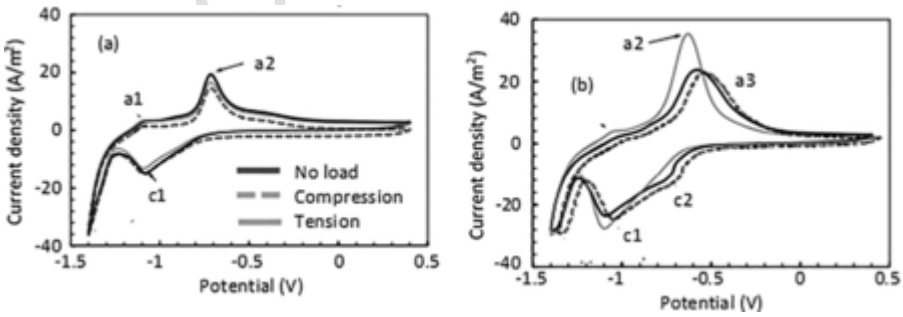

Fig. 2.5 Cyclic voltammograms recorded on C-ring electrodes (made of carbon steel) in (A) a NaCl-free solution, and (B) a solution containing 0.85M NaCl.
According to Y. Zhang, A. Poursaee, J. Mater. Civil Eng. 17 (8) (2015).

duction of compounds present in the passive film, namely:

- Peak a1 is attributed to the formation of $Fe(OH)_2$ and FeO
- Peak a2 is attributed to the reaction $Fe^{2+} \rightarrow Fe^{3+}$
- Peak a3 is attributed to an oxidation within the compact passive film (formation of Fe_2O_3, Fe_3O_4 and/or FeOOH)
- Peak c1 is related to the reduction reactions associated with the anodic peak a2
- Peak c2 is attributed to reduction reactions associated with the anodic peak a3

In the absence of chloride ions in the solution (Fig. 2.5A), there is no significant influence of either compressive or tensile stresses on the electrochemical response of the system. By contrast, large differences in electrochemical response were observed in the presence of chloride ions on carbon steel exhibiting tensile stresses in the elastic domain (Fig. 2.5B). For example, the current density at peak a2 (oxidation peak) is significantly increased. One reason could be the fact that chloride ions preferentially adsorb onto metallic surfaces in the presence of tensile stresses [46]. That passive film is then preferentially perturbed at locations where tensile stresses are present.

In literature, the deleterious influence of tensile stresses in the elastic domain was often attributed to changes in the electrical conductivity of passive films. The density of dopants increases significantly at increasing tensile stresses, as shown in Fig. 2.6 [40]. A linear relationship between the density of dopants and the level of tensile stress (in the elastic domain, was found for 316L stainless steel in alkaline solutions. The inner layer (density of acceptors) of the passive film in contact with the substrate is more affected by tensile stresses than the outer layer.

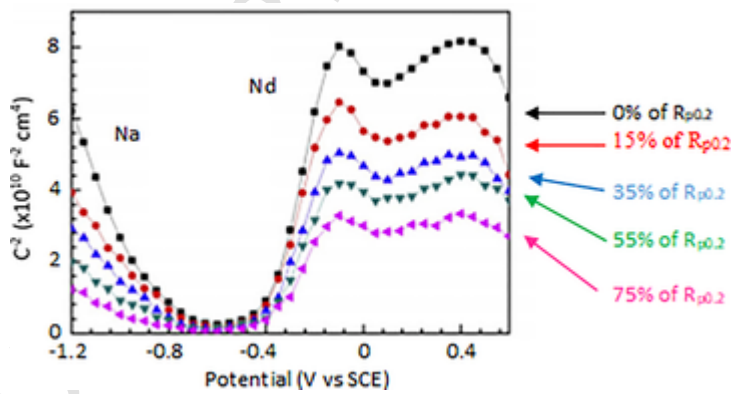

Fig. 2.6 Influence of tensile stress in the elastic domain on the Mott-Schottky plots of 316L stainless steel in 0.05M H_3BO_3 + 0.075M $Na_2B_4O_7 \cdot 10H_2O$ (buffered solution, pH 9.2). N_a is the density of acceptors and N_d is the density of donors.
According to L. Jinlong, L. Tongxiang, W. Chen, G. Ting, Mater. Sci. Eng. C 61 (2016) 32–36.

The evolution of the kinetic constants, k_0, of an oxidation reaction (mediator oxidation) at the 304L surface, was quantified by scanning electrochemical microscopy for various tensile stresses in the elastic domain [33]. k_0 significantly increased with increasing tensile stress, indicating that the reaction is promoted. According to the Point Defect Model [47], this phenomenon was ascribed to the acceleration of the transport of oxygen vacancies. This analysis is consistent with the experimental results obtained from the Mott-Schottky plots presented above.

Tensile stresses in the elastic domain may also affect the galvanic coupling between two metallic alloys. So, e.g., when aluminum alloy (AA5050) undergoes tensile stress after being coupled to 40CrNiMoA steel in 3.5% NaCl at 30°C for 20 h, corrosion was promoted [48]. With increasing stress, the potential of AA5050 decreases whereas the potential of steel remains more-or-less unchanged (Table 2.3). The potential difference between this aluminum alloy and 40CrNiMo steel (driving force for the galvanic coupling) then increases and thus promotes the galvanic coupling between the two alloys, ending up in the anodic dissolution of AA5050 (less noble alloy). The average current density (calculated over the 20 h of immersion) increases as the stress applied to the aluminum alloy increases (Table 2.3). It is increased by a factor of 2 at 75%$R_{p0.2}$ when to compared to the stress-free situation.

2.5 Influence of plastic deformation

Plastic deformation can be achieved by applying external loads like, e.g., uniaxial tensile tests, bending tests, extrusion tests, but also by surface preparation methods like, e.g., mechanical polishing, by elaboration methods, e.g., rolling, and by processing methods like, e.g., welding and cutting techniques. Applying loads in the plastic domain of the stress-strain curves may induce several changes in a metallic alloy, namely:

Table 2.3

Table 2.3 Galvanic corrosion potentials and current densities of AA5050 vs 40CrNiMoA steel.

	Galvanic corrosion potentials (mV vs SCE)		Average current density (µA/cm^2)
Stress	***Aluminum alloy***	***Steel***	
No stress	−775	−653	31.7
25%$R_{p0.2}$ Al	−890	−654	43.95
50%$R_{p0.2}$ Al	−912	−639	50.86
75%$R_{p0.2}$ Al	−923	−636	58.16

According to L. Jinlong, L. Tongxiang, W. Chen and G. Ting, Mater. Sci. Eng. C 61 (2016) 32–36.

- Formation of steps at the surface resulting from the emergence of slip bands,
- Activation of dislocations (both geometrically necessary (GND) and statistically stored dislocations (SSD)). GND accommodates nonuniform strains at the crystal scale. They are associated with the local incompatibility of the crystal lattice due to geometrical constraints. By contrast, SSD form by the random trappings of dislocations. Note that only GND induces changes of the lattice orientation and can be detected using diffraction-based techniques [49]. A large amount of GND may accumulate in the material to form geometrically necessary dislocation boundaries. Then SSD are stored between these geometrically necessary dislocation boundaries,
- Increase of the surface roughness,
- Grain refinement,
- Formation of microcracks, microvoids,
- Changes in the passive film properties (composition, structure, thickness).

These numerous changes can affect the electrochemical parameters in the plastic domain. In addition, synergistic effects between two or more of these parameters may occur and some parameters may have antagonistic effects. Therefore, the study of the influence of plastic deformation on the electrochemical response of metallic alloys is a difficult task. It is hard to propose quantitative relationships between plastic deformation and electrochemical parameters. The reason is that nonlinear evolutions are often found. In general plastic, deformation has a deleterious influence on the electrochemical processes and the corrosion resistance of metallic alloys [50–55]. The evolution of the amount of metastable pits (Fig. 2.7A) and electrical charge (Fig. 2.7B) vs. cold rolling reduction is shown in Fig. 2.7 [55]. In both cases, nonlinear relationships were found. It is worth mentioning that different laws were obtained for the two parameters. The amount of metastable pits increases with increasing cold rolling reduction up to 20% and then decreases. By contrast, the electrical charge increases continuously with the cold rolling reduction.

The effect of plastic deformation on the corrosion processes in aqueous media can be linked to geometrical effects, crevice effects, dislocations effects, and modifications of the passive film [55].

2.5.1 Geometrical effects due to the presence of slip bands

Numerous alloys have a crystallographic orientation-dependent corrosion behavior [56]. In this case, local techniques in physics and electrochemistry are powerful tools to investigate corrosion mechanisms. For example, Electron backscatter diffraction (EBSD) analyses can be coupled to local electrochemical measurements using microcapillary-based techniques. These techniques allow the selection and interrogation of single sites and are therefore becoming increasingly popular to investigate the electrochemical behavior of metallic grains/phases and nonmetallic heterogeneities in alloys. This methodology was applied to pure aluminum [57] to determine the corro-

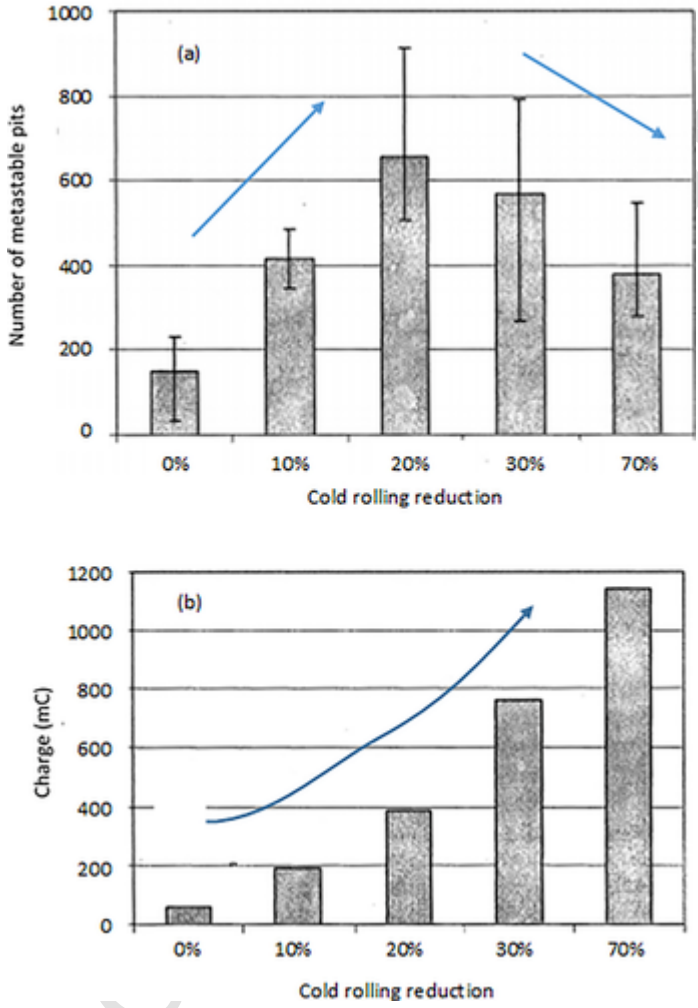

Fig. 2.7 Evolution of (A) the number of metastable pits and (B) electrical charge vs cold rolling reduction measured on 304 immersed at open circuit potential in a solution containing 0.1M NaCl + 2×10^{-4} M $FeCl_3$.
According to L. Peguet, B. Malki, B. Baroux, Corros. Sci. 49 (2007) 1933–1948.

sion behavior of individual grains whose crystallographic orientation was previously determined by means of EBSD.

It was revealed that pitting corrosion occurs after polishing along grains oriented along (111) planes. There is no pitting corrosion on grains oriented along (001) and (101) planes. For example, Fig. 2.8A shows polarisation curves obtained in several

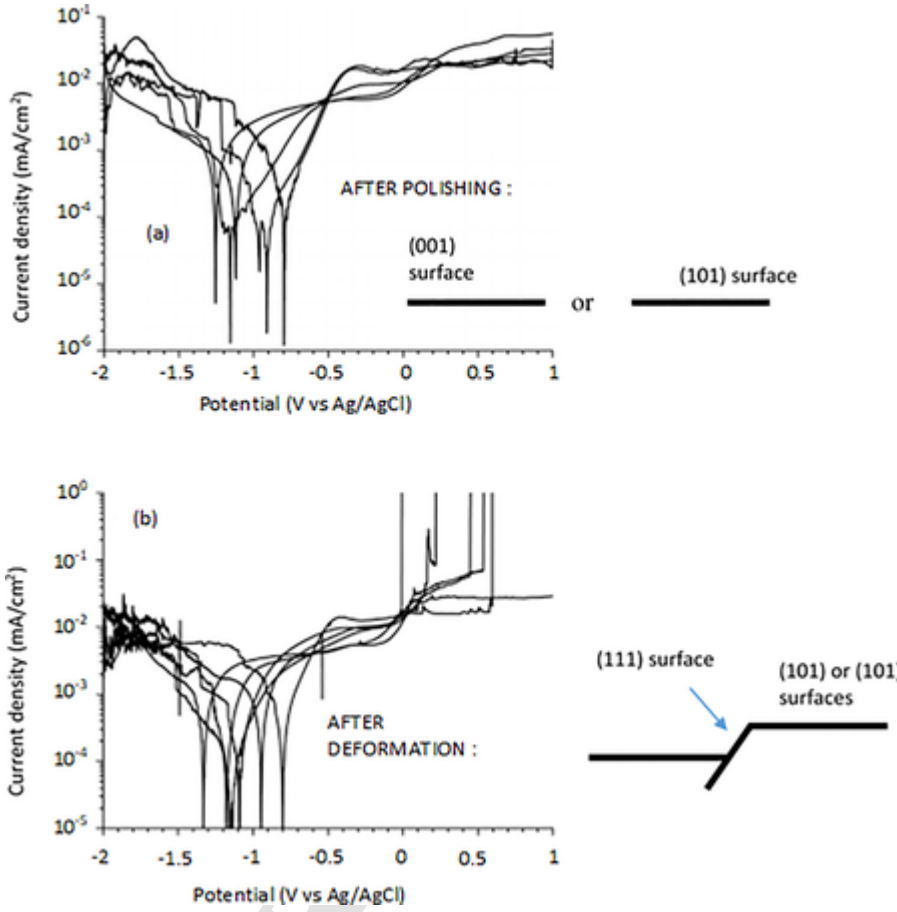

Fig. 2.8 Local polarisation curves of (001) grains of pure aluminium in 0.1M NaCl (A) after polishing and (B) a plastic deformation of 5.5%.
According to H. Krawiec, Z. Szklarz, Electrochim. Acta 203 (2016) 426–438.

(001) grains. In this case, a large passive range is observed and no pitting potential can be defined. The same behavior was obtained on (101) grains.

By contrast, pitting corrosion occurs on grains oriented along (001), (101), and (111) planes after plastic deformation of 5.5% (Fig. 2.8B showing polarisation curves in different (001) grains). This behavior was also observed on grains possessing a very low density of dislocations. It was proposed that pits initiate at steps generated by the emergence of slip bands at a material surface. Indeed, these steps are oriented along (111) planes (cubic system). This orientation exhibits the lowest corrosion resistance after polishing. Pitting potentials measured after deformation on

(001) and (101) grains are located within the same potential range as those measured on (111) oriented grains after polishing, confirming the previous assumption.

2.5.2 Crevice effect due to the presence of cracks

Microcracks and microvoids can be generated at material surfaces during plastic deformation. Depending on the geometry of these defects, a crevice effect may occur in aggressive environments. The presence of deep and narrow microcracks in Al-Cu4Mg1 alloy after plastic deformation induces a drop of the pitting potential in NaCl media [58]. The physical-chemical conditions in the microcracks promote the initiation and propagation of stable pits. A similar effect was observed in metallic alloys containing MnS-inclusions after plastic deformation [59–62]. The transition from metastable to stable pitting depends on the location of microcracks [61]. Stable pits are systematically observed in presence of microcracks located in the matrix (see a blue curve in Fig. 2.9). By contrast, only metastable pits were found when microcracks propagated along with the interface between matrix and inclusions (see a red curve in Fig. 2.9). The finite element method can be used to predict the location where microcracks initiate. The initiation depends on the mechanical properties of both the matrix and the inclusions, and the morphology of inclusions.

2.5.3 Modifications of the passive film

Changes in the electrochemical behavior of Ti6Al4V in the Ringer's solution at 37°C were associated with modifications of the chemical composition of the passive film

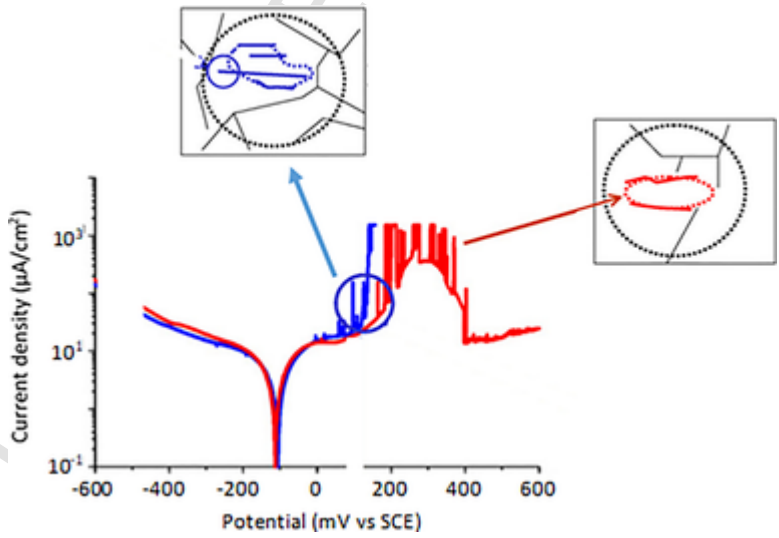

Fig. 2.9 Influence of the morphology of microcracks generated during plastic deformation (6%) on the local polarisation curves of 316L stainless steel containing MnS inclusions in 1M NaCl [61].

[63]. Auger measurements revealed that the beneficial influence of the presence of a mixed passive film composed of aluminum and titanium compounds is lowered after straining in the plastic domain (5%). The decrease of the quantity of aluminum in the passive film is associated with an increase of the current density in the passive range.

Changes in the structure of the passive film formed on pure iron [64], Ti6Al4Val-loy [65], and 304 stainless steel [66] were also considered to explain the influence of plastic deformation in the increase of corrosion susceptibility. The adsorption energy of oxygen on a Cu (100) surface affects the build-up of Cu_2O oxide films dependent on the stress applied to the substrate [67].

2.5.4 Presence of dislocations

During plastic deformation, GND and SSD are generated and dislocation structures are formed. The characteristics of dislocation structures depend on the deformation process and materials [68]. The density of dislocations can be calculated and the dislocations structures identified using transmission electron microscopy (TEM), for example. EBSD can also be used to locate regions with a density of GND. The presence of dislocation decreases the EWF value and therefore increases the corrosion susceptibility of metallic alloys [25].

Coupling local electrochemical measurements and the microstrain gauge technique, it was shown [69] that GND generated at some grain boundaries to accommodate incompatibilities play an important role in the kinetics of cathodic reduction reactions occurring on as-cast AlMg2 alloy after plastic deformation.

The kinetics of the hydrogen reduction reaction but also the recombination reactions can affect when the substrate is subjected to plastic deformation [70]. Such significant effects have been reported on single crystals and polycrystals of nickel in an H_2SO_4 environment. That clearly shows the competing effects associated with the expression of the deformation like dislocation density, stress, and the emergence of deformation bands.

Dislocations play also a crucial role in the initiation of stable pits in various metallic alloys immersed in NaCl-based media like, e.g., pearlitic alloys [71], duplex stainless steels [72]. In the case of pearlitic alloys in 0.05M NaCl (Fig. 2.10), a critical value of the grain orientation spread can be defined, leading to a drop of the pitting potential. Regarding Ta-4%W alloy after plastic deformation, pitting corrosion occurs at regions of original grain boundaries and dislocation boundaries (GNB) [73].

The influence of dislocations on the dissolution of polycrystalline nickel was studied in acidic environment [74, 75]. The thermodynamic approach showed that they could be the reason for the increase of the dissolution rate of the metal by modifying the adsorption sites for hydroxide species.

2.5.5 Influence of grain refinement generated by severe plastic deformation

Interested readers are referred to several review papers [76–78] describing the influence of grain refinement by severe plastic deformation (SPD) on corrosion. It is im-

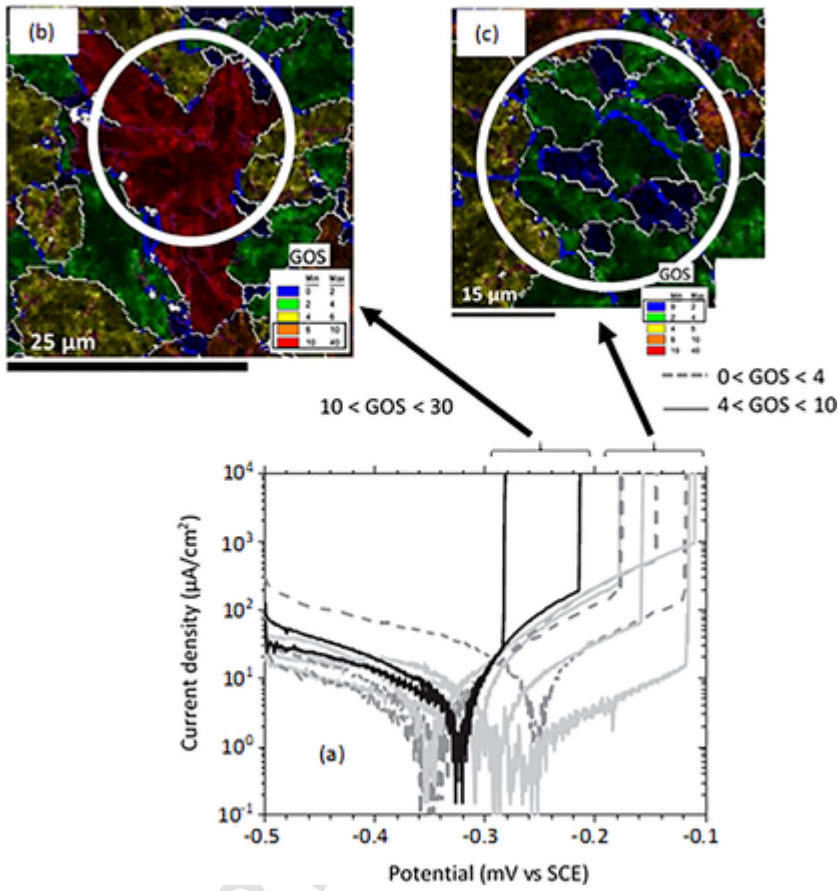

Fig. 2.10 (A) Local polarisation curves of pearlitic steel in 0.05M NaCl in sites with different GOS values. (B and C) Sites where electrochemical analysis were performed [71].

portant to keep in mind that changes observed in the corrosion behavior of alloys with fine/ultrafine grains are imparted by not only grain refinement but also other microstructural changes (absence of porosity, residual stresses, crystallographic orientation, and dislocation density).

A review of the literature [78] indicates that it seems likely that grain refinement (with other microstructural changes induced during refinement) does not compromise the overall corrosion resistance, and in many cases, improve it in comparison with coarse-grained alloys.

The impact of the presence of fine/ultrafine grains on the corrosion behavior of the main families of alloys can be classified as follows (in descending order of impact): stainless steels, followed by aluminum and magnesium alloys [78]. Table 2.4

Table 2.4

Table 2.4 Examples of corrosion behavior of alloys with fine/ultra-fine structure.

Alloys	Grain size	Corrosion tendency	Techniques	References
Al 7150	120 nm	=	High pressure torsion	[79]
Al 2024	200 nm	+	Equal channel angular pressing	[80]
AZ91D	[1; 2] µm	–	Equal channel angular pressing	[81]
AZ31B	523 nm	+	Ultrasonic peening	[82]
AISI316	20–70 nm	–	Hydraulic extrusion	[83]
Fe-20%Cr	200 nm	+	Equal channel angular pressing	[84]
AISI321	15 nm	=	Ultrasonic peening	[85]

reports some examples of corrosion tendency observed in some iron and aluminum alloys after grain refinement. In this Table, the corrosion behavior of the alloy with fine/ultrafine structure is compared to that of the same alloy with coarse structure: The sign "+" means better corrosion resistance of the fine structure whereas the sign "–" means worst corrosion resistance. The sign "=" is used when no significant changes are observed between the two structures. The impact is relatively marginal in pure copper and titanium alloys.

Processing involved in grain refinement can alter the bulk (including the surface) or only the surface of the alloy [78]. Grain refinement can be obtained throughout the volume of the alloy using different techniques, namely equal channel angular pressing (ECAP), high-pressure torsion (HPT), and accumulative roll bonding (ARB), for example. Grain refinement can also be obtained within a sublayer near the surface using various techniques like high power shot blast, ultrasonic peening, surface mechanical attrition treatment (SMAT), burnishing/brushing (under certain conditions), and friction stir processing. In this case, the volume properties are not altered by processing.

Depending on the alloy and experimental conditions used to refine the structure (type of technique and experimental conditions), the grain size ranges from the microscale (fine structures) down to the nanoscale (ultrafine structures). Table 2.4 gives some examples of grain size values.

Regarding tribocorrosion, grain refinement could enhance the wear resistance of materials by increasing the hardness [76, 86]. It could also enhance the tribocorrosion resistance of alloys mainly by increasing surface hardness and forming protective and lubricating surface layers [86]. Interested readers are referred to a review paper [86] describing the tribocorrosion behavior of nanocrystalline metals. In this paper, nanocrystalline metals are elaborated by means of surface deposition techniques. However, obtained results can be very useful to interpret the corrosion behavior of alloys after grain refinement by severe plastic deformation, as both materials (elaborated by surface deposition techniques and by severe plastic deformation) have comparable grain size. For example, it was noticed on nanocrystalline metals that under tribocorrosion conditions, the presence of a nanostructure could decrease or increase the corrosive rates (depending on the property of the passive and the nature of corrosion products).

Only a few papers investigate the influence of grain refinement (induced by severe plastic deformation) on the tribocorrosion of metals and alloys. This is the case of 304L stainless steel [87] and titanium [88]. In the latter case [87], a nanocrystallized surface layer of around 150-µm thickness was created by surface peening. Electron back-scattered diffraction (EBSD) has put in evidence an interesting point: the nanocrystalline surface layer was heterogeneous and composed of two sublayers. The upper layer consists of nanosized ferrite grains whereas the bottom layer was composed of martensite and deformed austenite.

Fig. 2.10 compares the corrosion and mechanical contributions of the total wear loss for the untreated and treated samples (304L stainless steel) [87]. Experiments were performed under continuous (Fig. 2.11A) and intermittent (Fig. 2.11B) sliding. For both sliding conditions and both samples, the mechanical wear contribution was predominant in the total wear loss. Tribocorrosion mechanism was dominated by abrasion mechanical removal of the uncovered surface.

In addition, the total wear loss measured on the treated sample is significantly lower than that of the untreated sample under intermittent sliding (Fig. 2.10B). Un-

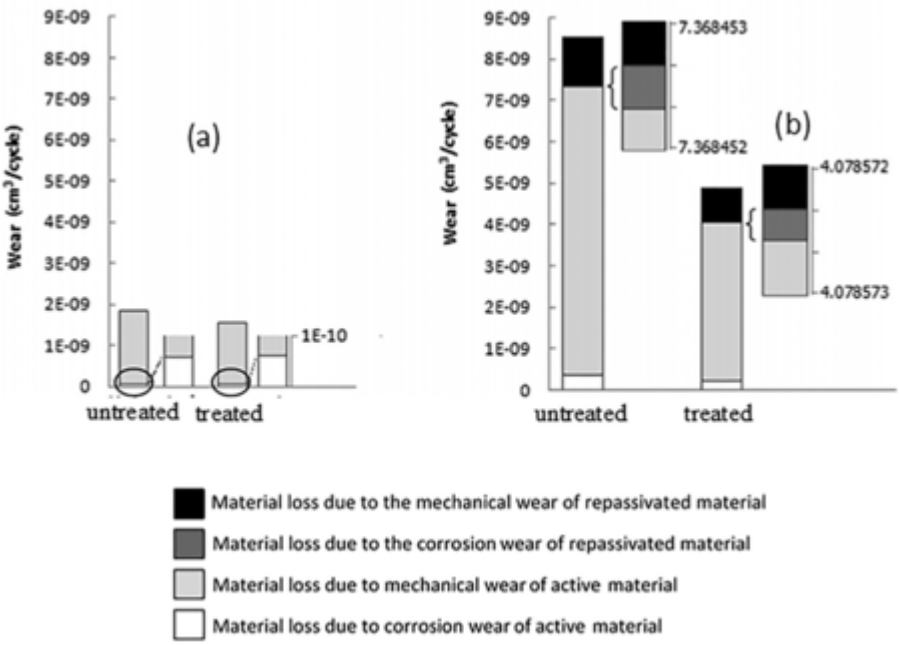

Fig. 2.11 Contribution of wears obtained on nanopeened AISI 304L under (A) continuous and (B) intermittent sliding against alumina pin (5 N, 0.0628 m/s) in filtrate olive pit/tap water.
According to F. Ben Saada, Z. Antar, K. Elleuch, P. Ponthiaux, N. Gey, Wear 394–395 (2018) 71–79.

der continuous sliding, the difference is very large. This shows that that the treated 304L was more sensitive to tribocorrosion under intermittent sliding than continuous one due to depassivation/repassivation phenomena. This also shows that the difference observed between both samples depends on sliding conditions.

2.6 Conclusions

There is an abundant bibliography on the interactions between mechanical stress/strain and the reactivity of metal alloys. The following conclusions can be drawn:

(1) Regarding the influence of compressive stresses, almost all publications show a positive impact on the electrochemical response and corrosion resistance of alloys. Some elements of response were provided for stainless steels considering the properties of passive films, namely changes in chemical composition.

(2) All publications show that tensile stresses in the elastic domain of stress-strain curves have a deleterious influence on the corrosion resistance of alloys. This is attributed to an increase in the conductivity of passive films.Several explanations were proposed to explain the influence of compressive and tensile stresses on the electrochemical response of metallic alloys, mainly changes in the electron work function and changes in the properties (composition and structure) of passive films.

(3) Effects obtained in the plastic domain of the stress-strain curves are very difficult to analyze. They depend on many parameters like the activation of several types of dislocations, the nature of the structure of dislocations, the emergence of slip bands, the surface roughness, and the presence of cracks. Nonlinear relationships between plastic deformation and electrochemical parameters are generally found.

2.7 Notations

k_0 kinetic constant of a reaction (m/s)
σ normal stress (Pa)
σ_{11} normal stress along the x_1-axis (Pa)
σ_{22} normal stress along the x_2-axis (Pa)
$R_{p0.2}$ apparent yield strength (Pa)
N_a density of acceptors in the passive film (m^{-2})
N_d density of donors in the passive film (m^{-2})

References

[1] V. Vignal, O. Devos, X. Feaugas, Effect of stress/strain fields on electrochemical activity: metallurgy/stress interaction and surface reactivity, in: C. Blanc, I. Aubert (Eds.), Mechanics—Microstructure—Corrosion Coupling: Concepts, Experiments, Modeling and Cases, ISTE Press Ltd and Elsevier Ltd, London/Kidlington Oxford, 2019, pp. 271–284.

[2] K. Pearson, Philos. Mag. 50 (1900) 157–175.

[3] O. Takakuwa, H. Soyama, Adv. Chem. Eng. Sci. 5 (2015) 62–71.

[4] P. Peyre, V. Vignal, Techniques de l'Ingénieur 1 (2012) COR 1 580.

[5] O. Hatamleh, P.M. Singh, H. Garmestani, Corros. Sci. 51 (2009) 135–143.

[6] U. Trdan, J. Grum, Investigation of corrosion behaviour of aluminium alloy subjected to laser shock peening without a protective coating, Adv. Mater. Sci. Eng. (2015) paper ID 705306.

[7] H. Amar, V. Vignal, H. Krawiec, C. Josse, P. Peyre, S.N. da Silva, L.F. Dick, Corros. Sci. 53 (2011) 3215–3221.

[8] P. Peyre, C. Carboni, Ann. Chim.–Sci. Mat. 29 (2004) 83–93.

[9] V. Vignal, N. Mary, C. Valot, R. Oltra, L. Coudreuse, Electrochem. Solid-State Lett. 7 (2004) C39–C42.

[10] T. Sano, A. Hirose, Rev. Laser Eng. 36 (2008) 91–92.

[11] N. Lisenko, C.D. Evans, Y.L. Yao, Manuf. Lett. 23 (2020) 5–8.

[12] X. Liu, G.S. Frankel, Corros. Sci. 48 (2006) 3309–3329.

[13] M. Salahshoor, Y.B. Guo, Surface integrity of biodegradable magnesium-calcium (Mg-Ca) alloy by low plasticity burnishing, Proc. of the STLE/ASME 2010 International Joint Tribology Conference, Paper No. IJTC2010-4121, 2010, pp. 61–63.

[14] S. Kanchidurai, P.A. Krishanan, K. Baskar, K. Saravana, R. Mohan, A review of inducing compressive residual stress—shot peening; on structural metal and welded connection, IOP Conf. Ser. Earth Environ. Sci. 80 (2017) paper 012033.

[15] R.K. Gupta, N. Prasad, A.K. Rai, R. Biswal, R. Sundar, A. Bose, P. Ganesh, K. Ranganathan, K.S. Bindra, R. Kaul, Corrosion study on laser shock peened 316L stainless steel in simulated body fluid and Chloride medium, Lasers Manuf. Mater. Process. 5 (2018) 270–282.

[16] V. Vignal, C. Valot, R. Oltra, M. Verneau, L. Coudreuse, Corros. Sci. 44 (2002) 1477–1496.

[17] F. Navai, J. Mater. Sci. 30 (1995) 1166–1172.

[18] F. Navai, O. Debbouz, J. Mater. Sci. 34 (1999) 1073–1079.

[19] V. Vignal, O. Delrue, O. Heintz, J. Peultier, Electrochim. Acta 55 (2010) 7118–7125.

[20] W. Li, M. Cai, Y. Wang, S. Yu, Scr. Mater. 54 (2006) 921–924.

[21] L. Chen, C. Shi, X. Li, Z. Mi, D. Wang, H. Liu, L. Qiao, Materials 10 (2017) paper 273.

[22] N. Fuertes Casals, A. Nazarov, F. Vucko, R. Pettersson, D. Thierry, J. Electrochem. Soc. 162 (2015) C465–C472.

[23] W. Li, D.Y. Li, J. Phys. D. Appl. Phys. 37 (2004) 948–951.

[24] W. Li, Y. Wang, D.Y. Li, Phys. Status Solidi 201 (2004) 2005–2012.

[25] W. Li, D.Y. Li, Mater. Sci. Technol. 18 (2002) 1057–1060.

[26] B. Łosiewicz, M. Popczyk, M. Szklarska, A. Smołka, P. Osak, A. Budniok, Solid State Phenom. 228 (2015) 369–382.

[27] S. Liu, H. Lu, D.Y. Li, Appl. Surf. Sci. 351 (2015) 316–319.

[28] Y. Li, D.Y. Li, Appl. Phys. Lett. 95 (2004) 7961–7965.

[29] R.K. Zhu, J.L. Luo, Electrochem. Commun. 12 (2010) 1752–1755.

[30] X. Feng, Y. Zuo, Y. Tang, X. Zhao, X. Lu, Electrochim. Acta 58 (2011) 258–263.

[31] S.J. Kim, Int. J. Hydrog. Energy 42 (2017) 19367–19375.

[32] K.R. Trethewey, M. Paton, Mater. Lett. 58 (2004) 3381–3384.
[33] D. Sidane, O. Devos, M. Puiggali, M. Touzet, B. Tribollet, V. Vivier, Electrochem. Commun. 13 (2011) 1361–1364.
[34] W.J. Yang, P. Yang, X.M. Li, W.L. Feng, Mater. Corros. 63 (2012) 401–407.
[35] Y. Zhang and A. Poursaee, J. Mater. Civil Eng. 2015, 27, n°8.
[36] J. Zhang, J. Liu, Q.H. Huang, Z.Y. Cheng, J.T. Guo, Anti-Corros. Method Mater. 62 (2015) 103–108.
[37] M. Dollah, M.J. Robinson, Corros. Eng. Sci. Technol. 46 (2011) 42–48.
[38] P.J.E. Forsyth, Mater. Lett. 41 (1999) 173–180.
[39] Y. Wang, K.Y. Lib, F. Scenini, J. Jiao, S.J. Qu, Q. Luo, J. Shen, Surf. Coat. Technol. 302 (2016) 27–38.
[40] L. Jinlong, L. Tongxiang, W. Chen, G. Ting, Mater. Sci. Eng. C 61 (2016) 32–36.
[41] W. Ding, Y. Liu, J. Xie, L. Sun, T. Liu, F. Yuan, J. Pan, Metals 9 (2019) 709.
[42] G. Zhu, S. Wang, W. Cheng, G. Wang, W. Liu, Y. Ren, Coatings 9 (2019) 578.
[43] H. Jiang, L. He, Z. Ren, F. Shao, S. Yuan, Int. J. Adv. Manuf. Technol. 106 (2020) 4693–4705.
[44] J. Chen, Q. Fang, L. Zhang, Int. J. Adv. Manuf. Technol. 75 (2014) 615–627.
[45] L. Bai, K. Jiang, L. Gao, Mater. Res. 21 (2018) e20180166.
[46] V. Vignal, H. Zhang, O. Delrue, O. Heintz, I. Popa, J. Peultier, Corros. Sci. 53 (2011) 894–903.
[47] D.D. Macdonald, Russ. J. Electrochem. 48 (2012) 235–258.
[48] T. Cui, D. Liu, P. Shi, J. Liu, Y. Yi, H. Zhou, J. Wuhan Univ. Technol. Mater. Sci. Ed. 33 (2018) 688–696.
[49] T. Leffers, T. Lorentzen, The plastic regime, including anisotropy effects, in: M.T. Hutchings, A.D. Krawitz (Eds.), Measurement of Residual and Applied Stress Using Neutron Diffraction, NATO ASI Series, Series E. Applied Sciences 216, 1992, pp. 171–187.
[50] A.H. Ramirez, C.H. Ramirez, I. Costa, J. Braz. Chem. Soc. 25 (2014) 1270–1274.
[51] V. Tandon, A.P. Patil, R.C. Rathod, S. Shukla, Mater. Res. Express 5 (2018) 026528.
[52] B. Mazza, P. Pedeferri, D. Sinigaglia, A. Cigada, G.A. Mondora, G. Re, G. Taccani, D. Wenger, J. Electrochem. Soc. 126 (1979) 2075–2081.
[53] H.B. Li, Z.H. Jiang, Q.F. Ma, Z. Li, Adv. Mater. Res. 217–218 (2011) 1180–1184.
[54] M. Rifai, H. Miyamoto, H. Fujiwara, Mater. Sci. Appl. 5 (2014) 568–578.
[55] L. Peguet, B. Malki, B. Baroux, Corros. Sci. 49 (2007) 1933–1948.
[56] T.Q. Ansari, J.L. Luo, S.Q. Shi, Mater. Degrad. 3 (2019) 1–12.
[57] H. Krawiec, Z. Szklarz, Electrochim. Acta 203 (2016) 426–438.
[58] H. Krawiec, V. Vignal, Z. Szklarz, J. Solid State Electrochem. 13 (2009) 1181–1191.
[59] N. Shimahashia, I. Muto, Y. Sugawara, N. Hara, J. Electrochem. Soc. 161 (2014) C494–C500.
[60] E.G. Webb, T. Suter, R.C. Alkire, J. Electrochem. Soc. 148 (2001) B186–B195.
[61] R. Oltra, V. Vignal, Corros. Sci. 49 (2007) 158–165.
[62] Z. Szklarska-smialowska, Corrosion 28 (1972) 388–396.
[63] H. Krawiec, V. Vignal, J. Loch, P. Erazmus-Vignal, Corros. Sci. 96 (2015) 160–170.
[64] T. Yamamotoz, K. Fushimi, S. Miura, H. Konno, J. Electrochem. Soc. 157 (2010) C231–C237.
[65] D. Nakhaie, A. Davoodi, G.R. Ebrahimi, Corrosion 72 (2016) 110–118.
[66] T. Souier, M. Chiesa, Effect of surface conditions and strain hardening on the passivity breakdown of 304 stainless steel, J. Mater. Res. 27 (2012) 1580–1588.
[67] D. Kramer, Y. Wang, J. Wharton, Faraday Discuss. 180 (2015) 137–149.
[68] D.A. Hughes, N. Hansen, D.J. Bammann, Scr. Mater. 48 (2003) 147–153.
[69] H. Krawiec, V. Vignal, Z. Szklarz, Corros. Sci. 65 (2012) 387–396.
[70] H. El Alami, J. Creus, X. Feaugas, Electrochim. Acta 51 (2006) 4716–4727.
[71] V. Rault, V. Vignal, H. Krawiec, F. Dufour, Corros. Sci. 100 (2015) 667–671.
[72] V. Vignal, D. Ba, H. Zhang, F. Herbst, S. Le Manchet, Corros. Sci. 68 (2013) 275–278.

[74] M. Sahal, J. Creux, R. Sabot, X. Feaugas, Acta Mater. 54 (2006) 2157–2167.
[75] M. Sahal, C. Savall, J. Creus, R. Sabot, X. Feaugas, Dislocations effect on kinetic of passivation of polycrystalline nickel in H2SO4 medium, in: P. Marcus, V. Maurice (Eds.), Passivation of Metals and Semiconductors, and Properties of Thin Oxide Layers, Elsevier, 2006, pp. 519–524.
[76] K.D. Ralston, N. Birbilis, Corrosion (2010) 66 075005-075005-13.
[77] E. Karakulak, J. Magnes. Alloy 7 (2019) 355–369.
[78] H. Miyamoto, Mater. Trans. 57 (2016) 559–572.
[79] K.S. Ghosh, N. Gao, M.J. Starink, Mater. Sci. Eng. A 552 (2012) 164–171.
[80] J.G. Brunner, N. Birbilis, K.D. Ralston, S. Virtanen, Corros. Sci. 57 (2012) 209–214.
[81] D. Song, A.B. Ma, J.H. Jiang, P.H. Lin, D.H. Yang, J.F. Fan, Corros. Sci. 53 (2011) 362–373.
[82] Z. Pu, G.L. Song, S. Yang, J.C. Outeiro, O.W. Dillon Jr., D.A. Puleo, I.S. Jawahir, Corros. Sci. 57 (2012) 192–201.
[83] M. Pisarek, P. Kedzierzawski, M. Janik-Czachor, K.J. Kurzydlowski, Corrosion 64 (2008) 131–137.
[84] M. Rifai, H. Miyamoto, H. Fujiwara, Int. J. Corros. 386865 (2015) 1–9.
[85] B.N. Mordyuk, G.I. Prokopenko, M.A. Vasylyev, M.O. Iemov, Mater. Sci. Eng. A 458 (2007) 253–261.
[86] Z. Wang, Y. Yan, L. Qiao, Mater. Trans. 56 (2015) 1759–1763.
[87] F. Ben Saada, Z. Antar, K. Elleuch, P. Ponthiaux, N. Gey, Wear 394–395 (2018) 71–79.
[88] S. Faghihi, D. Li, J.A. Szpunar, Nanotechnology 21 (2010) 485703.